BNL-29774

CONF-810747--1

MASTER

HYPERNUCLEI AND INTERACTIONS OF KAONS WITH NUCLEI

Carl B. Dover

DISCLAIMER

The submitted manuscript has been authored under contract DE-AC02-76CH00016 with the U.S. Department of Energy. Accordingly, the U.S. Government retains a nonexclusive, royalty-free license to publish or reproduce the published form of this contribution, or allow others to do so, for U.S. Government purposes.

Talk given at the 9th International
Conference on High Energy Physics and
Nuclear Structure at Versailles, France,
July 6-10, 1981.

BNL-29774

HYPERNUCLEI AND INTERACTIONS OF KAONS WITH NUCLEI

Carl B. DOVER

Brookhaven National Laboratory
Upton, New York, USA 11973

Abstract: Recent experimental and theoretical progress in hypernuclear physics is reviewed. Different models for hyperon-nucleus central and spin-orbit potentials are compared: several models yield a very small spin-orbit strength for the Λ, as experimentally observed, but differ considerably in their predictions for the Σ. The new data on the $^{13}_{\Lambda}C$ hypernuclear spectrum, as obtained in the (K^-,π^-) strangeness exchange reaction at 800 MeV/c, are discussed. We show how one extracts constraints on the Λ-nucleus and effective Λ-nucleon interactions from the data. The new BNL data on the (K^-,π^+) reaction at 720 MeV/c, leading to Σ-hypernuclear states, are examined. We elucidate the case of $^6Li(K^-,\pi^+)^6_{\Sigma}H$ in some detail, and also present some speculations concerning the (K^-,π^+) reaction on other targets. We analyze the physical mechanisms which may lead to unusually narrow Σ excitations in some systems. Finally, we review the physics motivations for several future hypernuclear experiments which are already under development, such as $(K^-,\pi^-\gamma)$ and $(\pi^{\pm},K^+)$ studies, or under preliminary consideration, for instance, the (K^-,K^+) reaction producing S=-2 hypernuclei.

1. Introduction

There are several excellent reviews of hypernuclear physics in the literature, for instance those due to Cal[1], Povh[2] and, more recently, Dalitz[3]. Other aspects of kaon interactions with nucleons and nuclei have also been surveyed[4]. The present review essentially updates that of Dalitz[3] at the Berkeley conference, to include a discussion of the new data on Λ and Σ hypernuclei and their theoretical interpretation, as well as an appraisal of some of the future prospects for kaon physics. We treat the following topics: i) the theory of hyperon-nucleus single particle potentials, ii) constraints on the Λ-nucleon residual interaction and Λ-nucleus single particle potential from the spectroscopy of $^{13}_{\Lambda}C$, iii) interpretation of the new data on Σ hypernuclear states seen in the (K^-,π^+) reaction, including a discussion of the mechanisms which lead to narrow Σ states, iv) future prospects for hypernuclear physics via the study of $(K^-,\pi^-\gamma)$, $(\pi^{\pm},K^+)$, and (K^-,K^+) reactions, as well as weak decay modes.

2. Hyperon-nucleus single particle potentials

From an analysis of the $^{16}O(K^-,\pi^-)^{16}_{\Lambda}O$ reaction at 715 MeV/c, the CERN group[5] arrived at the conclusion that the one-body spin-orbit potential for a Λ in the nucleus is at least an order of magnitude smaller than that for a nucleon. The essence of the argument is that the two strongest states seen in $^{16}_{\Lambda}O$ at 0° must correspond to the coherent $(nP^{-1}_{3/2}\otimes_{\Lambda}P_{3/2})_{0^+}$ and $(nP^{-1}_{1/2}\otimes_{\Lambda}P_{1/2})_{0^+}$ excitations, since the momentum transfer q is small (≈40 MeV/c). Because these peaks are observed to be separated by 6 MeV, which is attributable to the nucleon spin-orbit splitting in ^{16}O, it is concluded that the Λ spin-orbit potential must be small. The argument was made more quantitative by Bouyssy[6], who used the observed separation energy ΔE between the two 0^+ states and their relative intensity N to derive the difference $V_{LS}^{N}-V_{LS}^{\Lambda}$ of spin-orbit well depths, given a model for the ΛN residual interaction, which weakly admixes the two states. If we write the baryon-nucleus potential in the form

$$V_B(r) = V_B\, f_o(r) + V_{LS}^{B} \left(\frac{\hbar}{m_\pi c}\right)^2 \frac{1}{r}\frac{df_{LS}(r)}{dr}\ \vec{\ell}\cdot\vec{\sigma}_B \tag{1}$$

where $f_{o,LS}(r)$ are Woods-Saxon radial forms $\left(1+\exp(r-R_{o,LS})/a_{o,LS}\right)^{-1}$, with $R_{o,LS}=\{r_o, r_o^{LS}\}(A-1)^{1/3}$ and $B=\{N,\Lambda,\Sigma,\Xi\}$, we find[6]

$$V_{LS}^{N} - V_{LS}^{\Lambda} = 9.8 \pm 1.3 \text{ MeV} \tag{2}$$

Since $V_{LS}^{N} \sim 9.5$ MeV is required to fit the $P_{1/2}$-$P_{3/2}$ spin-orbit splitting for the nucleon in ^{16}O (assuming $r_o^{LS}=1.1$ fm, $a_{LS}=0.65$ fm), Eq. (2) indicates that V_{LS}^{Λ} is on the order of 1 MeV or less.

There have been several theoretical attempts [7-10] to understand the small size of the Λ spin-orbit coupling. Pirner[7] has used quantum chromodynamics (QCD) to estimate the average baryon-nucleus spin-orbit potential from the combined exchange of a quark and gluon between the baryon and the core nucleon. He obtains the ratios $V_{LS}^{N}:V_{LS}^{\Lambda}:V_{LS}^{\Sigma}=1:0:4/3$. Note that a large spin-orbit potential is predicted for the Σ. Recently, it has been pointed out by G. E. Brown[11] that the interchange of quarks required for color conservation generates an additional factor P_x (space-exchange operator) in the potential, which has been omitted by all previous authors. Since the one-body spin-orbit potential arises mostly from the two-body relative P-wave, we should use $P_x=-1$. Thus one predicts a nucleon spin-orbit potential of the <u>wrong sign</u>. It is then doubtful that the relative strengths V_{LS}^{B} have any significance.

The other attempts[8-10] to explain the small V_{LS}^{Λ} value use various extensions of the relativistic mean field theory (MFT) developed for ordinary nuclei by Walecka and his collaborators[12]. Noble[8] uses the MFT to predict V_{LS}^{Λ}, fixing the parameters for the hypernuclear case to reproduce the central well depth $V_\Lambda=30$ MeV. He includes only the scalar (ε) and vector (ω) meson exchanges shown in Fig. 1, and neglects the other graphs. The contribution of ω exchange contains two parts, due to vector coupling $(ig\bar{\psi}\gamma_\mu\psi\phi_\mu)$ and tensor coupling $\frac{f}{4m_N}\bar{\psi}\sigma_{\mu\nu}\psi(\partial^\mu\phi^\nu-\partial^\nu\phi^\mu)$

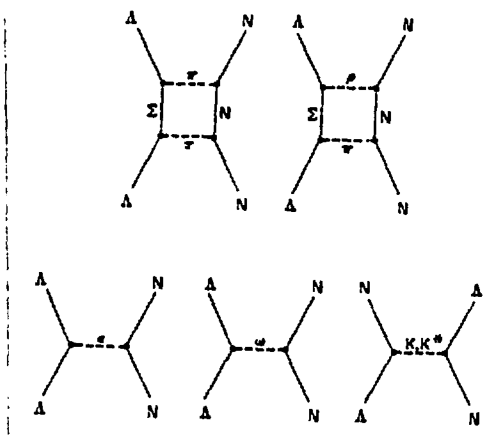

Fig. 1 Meson exchange processes which contribute to the ΛN interaction.

In the quark model, the ratio f/g is related to the anomalous moment of the baryon: for the Λ, we have $(f/g)_{\Lambda\Lambda\omega}=\frac{m_\Lambda}{m_N}\mu_\Lambda \simeq -0.73$. Noble observes that the tensor coupling contribution to V_{LS}^{Λ} tends to <u>cancel</u> the usual Thomas part of the interaction, leading to a small value[8] $V_{LS}^{\Lambda} \simeq 1.5 \pm 0.4$ MeV. A similar calculation in the context of MFT was done by Bouyssy[9], who also considered the Σ potential. In the latter case, the tensor coupling enhances V_{LS}^{Σ}, since $(f/g)_{\Sigma\Sigma\omega}=+0.58$ in the quark model. Bouyssy[9] obtains $V_{LS}^{\Lambda} \simeq 0.4$, $V_{LS}^{\Sigma} \simeq 7$, $V_{LS}^{N} \simeq 10$ MeV.

Brockmann and Weise[10] used a different approximation to obtain an estimate of the ratio

$V_{LS}^{\Lambda}/V_{LS}^{N}$. They include only the second order $\pi\pi$ and $\pi\rho$ exchange graphs, with intermediate Σ and $\Sigma(1385)$ excitations, plus the K and K^* exchanges. They omit the one boson ϵ and ω exchange graphs, which are assumed to be only phenomenological representations of the second order $\pi\pi(\epsilon)$ and $\pi\rho(\omega)$ processes. A comparison of these graphs with the corresponding terms for a nucleon, with N and $\Delta(1236)$ intermediate states, yields the rough estimate $V_{LS}^{\Lambda}/V_{LS}^{N}\approx 1/3$. In comparing N and Σ intermediate states, this reduction factor for the Λ is just $(g_{\Lambda\Sigma\pi}/g_{NN\pi})^2=(2\alpha_{PS}/\sqrt{3})^2$ in SU(3); the pseudoscalar F/D ratio is $\alpha_{PS}\approx 1/2$. For $\Delta(1236)$ and $\Sigma(1385)$, we also obtain a factor $(f^*_{\pi\Lambda\Sigma^*}/f^*_{\pi N\Delta})^2\approx(0.5\text{-}0.6)^2$, where f^* is a coupling strength obtained from the decay width of each resonance.

The MFT calculations[8-10] of hyperon-nucleus potentials, although appealingly simple and easy to interpret, have several drawbacks. The main problem is that the effects of short range repulsive correlations are omitted (in the Hartree approximation, one simply assumes a Yukawa form $\exp(-\mu r)/\mu r$ down to $r=0$). The ϵ and ω exchange terms contributing to the central potential are individually very large, although it is arranged that their sum produces the phenomenological well depth. Fock terms from π and ρ exchange, which are neglected, would contribute a large repulsive term to V_N. The important role of correlations in stabilizing relativistic calculations for the nucleon potential has been emphasized by Shakin and his collaborators[13]. So far the relativistic approach with correlations has not been worked out for hyperons, although this is an important program for the future.

Within the non-relativistic approximation, correlation effects have recently been included in a one boson exchange (OBE) picture of hyperon central, spin-orbit and isospin potentials[14]. The Moszkowski-Scott (MS) method[15] is used to derive an effective nucleon-nucleon or hyperon-nucleon interaction G from the free-space OBE potential. Thus the close connection between the free space two-body problem and the many-body potential (lost in the MFT approach) is preserved. The two-body potentials are taken from the OBE model of deSwart and collaborators[16], who impose SU(3) constraints on coupling constants in a simultaneous fit to all NN and YN data. Exchanges of nonets of scalar $(\delta,\epsilon,S^*,\kappa)$, pseudoscalar (π,η,η',K) and vector (ρ,ω,ϕ,K^*) mesons are included. Two versions of the model (D and F) are considered [14]. In Model D, the ϵ meson is treated as an SU(3) singlet, while in Model F, ideal mixing is used for the scalar nonet. Hard cores are used to parametrize short distance behavior; in Model F, although not in D, SU(3) constraints are applied to the core radii r_c as well as to coupling constants. The phenomenological ratios f/g of tensor to vector couplings for vector mesons required to fit the data differ considerably, particularly for Model D, from the SU(6) limit used in refs.[8,9].

The MS method[15] consists in using part of the intermediate range attraction $(r_c<r<r_0)$ to cancel the repulsive phase shift produced by the hard core. The resulting interaction G, corresponding essentially to a Yukawa form cut off for $r<r_0$, has a much smaller volume integral (typically 1/10) than the unmodified interaction used in the MFT. The various individual terms which contribute to the single particle potentials are thus much smaller when short range correlations are included, and the calculations are more stable with respect to small changes of the parameters. For channels where the interaction is net repulsive, the free Fermi-averaged t-matrix is used for G.

The two-body potentials for $r>r_c$ have the form[16]

$$V(r) = V_c(r) + V_\sigma \underset{\sim}{\sigma}_1\cdot\underset{\sim}{\sigma}_2 + V_T S_{12} + V_{LS}\underset{\sim}{L}\cdot\underset{\sim}{S}_+ + V_{ALS}\underset{\sim}{L}\cdot\underset{\sim}{S}_- \qquad (3)$$

where S_{12} is the usual tensor operator and $\underset{\sim}{S}_\pm=1/2(\sigma_1\pm\sigma_2)$. The new feature which appears for the YN system is the antisymmetric spin-orbit term $\underset{\sim}{L}\cdot\underset{\sim}{S}_-$, which vanishes for NN because of charge independence. We have not included the isospin dependence explicitly in Eq. (3); for isovector (π,ρ,δ) and strange (K,K^*,κ) exchanges, there are isospin factors $\underset{\sim}{\tau}_1\cdot\underset{\sim}{\tau}_2$ and $(1+\underset{\sim}{\tau}_1\cdot\underset{\sim}{\tau}_2)$, respectively. For Λ and Σ, the net spin-orbit potential is determined by the interplay between V_{LS} and V_{ALS}. In the non-relativistic model, we find for the dominant ω and ϵ

contributions to the YN system

$$\frac{V^{\omega}_{ALS}}{V^{\omega}_{LS}} \approx \frac{\left[(f/g)_{YY\omega} - (f/g)_{NN\omega}\right] (m_Y/m_N)^{1/2}}{3/2 + (f/g)_{NN\omega} + (m_Y/m_N)^{1/2} (f/g)_{YY\omega}} \tag{4}$$

$$\frac{V^{\varepsilon}_{ALS}}{V^{\varepsilon}_{LS}} \approx -(m_Y^2-m_N^2)/2m_N m_Y \approx \begin{cases} -0.17 & (\Lambda) \\ -0.24 & (\Sigma) \end{cases}$$

Note that in the quark model, we relate f/g to isoscalar anomalous moments so $(f/g)_{BB\omega}=\mu m_B/m_N$=(-0.12, -0.73, 0.58) for B=N,Λ,Σ, respectively. Thus we find that V^{ω}_{ALS} tends to cancel V^{ω}_{LS} for the Λ, where the two terms add coherently for the Σ. This is equivalent to the tensor coupling effect discussed by Noble[8] and Bouyssy[9]. In the deSwart models[16], the sign of this effect is preserved, although the tensor couplings are chosen to be consistent with SU(3) but not SU(6): we have[16] $(f/g)_{\Lambda\Lambda\omega}$={-0.122, -0.538} and $(f/g)_{\Sigma\Sigma\omega}$={1.417, 0.753} in Models D and F, respectively. Model D is seen to exhibit significant differences from the SU(6) limit (note, however, that the NN and YN data cannot be fit in this limit!)

Given the effective interaction G constructed from the sum $\sum_i V_i(r)$ of OBE exchanges, the one-body potential of Eq. (1) is obtained by a convolution of G with the nuclear density ρ(r):

$$V_B(r) = \int \rho(\underset{\sim}{r}')G(\underset{\sim}{r}-\underset{\sim}{r}')d^3\underset{\sim}{r}' \tag{5}$$

For nucleons, Fock terms are also included; for N, Σ and Ξ, an isospin decomposition of the well depths V_B and V^B_{LS} is also performed:

$$\begin{aligned} V_B &= -V_{OB} + V_{1B}\, \underset{\sim}{t}_B\cdot \underset{\sim}{T}/A \\ V^B_{LS} &= V^B_{LS0} + V^B_{LS1}\, \underset{\sim}{t}_B\cdot \underset{\sim}{T}/A \end{aligned} \tag{6}$$

For the YN system, there are strong couplings of the ΛN and ΣN channels, the most important of which is due to the tensor force ($^3S_1$-$^3D_1$, isospin I=1/2). The tensor potential also contributes important diagonal (ΣN→ΣN and YN→YN) couplings of $^3S_1$ and $^3D_1$ waves. In the present approach[14], these are included as second order effective potentials $-8V_T^2(r)/\Delta$ in the two-body problem, where the energy denominators Δ are adjusted in each channel to reproduce the exact coupled channel calculation of deSwart et al[16]. The second order tensor terms are also included in the central potential of Eq. (6), but omitted in the spin-orbit potentials quoted later. Scheerbaum[17] has shown that second order tensor terms give rise to about 1/3 of the nucleon-nucleus spin-orbit potential in heavy nuclei; we anticipate a similar effect for hyperons.

The results for the N, Λ and Σ central potentials are discussed in detail in ref.[14], and compared with other recent calculations[18-20]. A byproduct of the calculation is a quantitative understanding of the origin of the nucleon's isospin (Lane) potential: most of V_{1N} is found to arise from π and ρ Fock terms and second order tensor contributions involving ππ and πρ. Contrary to the assumption of the MFT approach[12], only a relatively small part of V_{1N} arises from the direct ρ exchange (Hartree) term. Since V_{1N} arises essentially from exchange and second order processes, it is predicted[21] to decrease strongly as the nucleon energy increases. There is now experimental evidence[22] for this effect in the preferential excitation of the Gamow-Teller spin-isospin mode over isobaric analogue states in the (p,n) reaction on nuclei at 160 MeV. One also predicts a significant Lane potential for the Σ: in Model D, we obtain[14] $V_{1\Sigma}\approx$55 MeV, while Dabrowski and

Rozynek[19] obtain 60 MeV.

The results for the isoscalar spin-orbit well depths in Models D and F are as follows[14] (in MeV):

$$V^{N}_{LSO} = 7.3(D),\ 8.8(F)$$
$$V^{\Lambda}_{LSO} = 1.9(D),\ 1.7(F) \qquad (7)$$
$$V^{\Sigma}_{LSO} = 2.9(D),\ 2.4(F)$$

The main contributions to V^{N}_{LSO} are from ω (4.3 MeV), ε(1.35 MeV) and ρ(1.35 MeV) exchanges (Model D). The latter is entirely a Fock term, while the ω and ε pieces include a factor 3/2 from antisymmetrization. The ρ exchange term and the 3/2 are omitted by Bouyssy[9], who thereby overestimates the ratio $V^{\Lambda}_{LSO}/V^{N}_{LSO}$. Note that both V^{Λ}_{LSO} and V^{Σ}_{LSO} are rather small; V^{Σ}_{LSO} is due almost entirely to ω(2.36 MeV) and ε(0.45 MeV) exchange, with very small contributions from ϕ, K and K^*. For V^{Λ}_{LSO}, the K and K^* terms are larger (-0.35 and 0.61 MeV) but tend to cancel, and ω(0.58 MeV) and ε(0.52 MeV) produce most of the net value of V^{Λ}_{LSO}.

These results suggest that a OBE model with SU(3) symmetry is capable of explaining both the two-body NN and YN data and the single particle properties of nucleons and hyperons in nuclei. The results of Eq. (7) for V^{B}_{LSO} are very similar for Models D and F, even though the scalar nonet is treated quite differently in the two models. In particular, the small value of V^{Λ}_{LSO} is not inconsistent with treating the ε as an SU(3) singlet.

3. Recent progress in Λ hypernuclear spectroscopy

The most recent data on the production of hypernuclei involve the non spin-isospin saturated targets ^{13}C, ^{14}N and ^{18}O. The (K^-,π^-) reaction on these targets at 800 MeV/c was studied at the Brookhaven AGS. The data[23] for $^{13}_{\Lambda}C$ at $\theta_L=0°$ at 15° are shown in Figs. 2 and 3. In contrast to spectra reported earlier[5,24] for closed shell targets such as ^{12}C and ^{16}O, the spectrum of $^{13}_{\Lambda}C$ displays a greater richness of peaks as well as a marked angular dependence. The energy resolution in this experiment is 2.5 MeV, so each peak in Figs. 2 and 3 represents a number of unresolved hypernuclear levels.

A comprehensive shell model for light hypernuclei, including core excitations and the effects of the ΛN residual interactions, has recently been developed[25] and applied to $^{13}_{\Lambda}C$ as a first example. The calculations are done in the distorted wave impulse approximation (DWIA), using phenomenological Woods-Saxon optical potentials to generate the K^- and π^- distorted waves. The parameters of the potential are adjusted to fit the available K^- and π^- elastic scattering data[26] on ^{12}C at the same momentum. A Fermi-averaged $K^-n\to\pi^-\Lambda$ amplitude in the lab system is used in the transition matrix element. Another ingredient is the choice of neutron and Λ bound state wave functions. These were generated from Woods-Saxon potentials whose geometry was chosen to be consistent with electron scattering charge distributions and neutron/proton single particle energies. Binding energies of (0.6, 0.1) MeV were used for the Λ in the $p_{3/2}$ and $p_{1/2}$ orbits, reflecting a small spin-orbit potential.

The differential (K^-,π^-) cross section for a transition $\alpha_i J_i T_i \to \alpha_f J_f T_f$ involving the single particle orbitals $\ell_N \to \ell_\Lambda$ is proportional to the sum

$$\sum_{\Delta L} \begin{pmatrix} \ell_N & \Delta L & \ell_\Lambda \\ 0 & 0 & 0 \end{pmatrix}^2 |M^{(\Delta L)}(q)|^2 \left(\alpha_f J_f T_f \middle\| \left(a^{+}_{\ell_\Lambda} \tilde{a}_{\ell_N}\right)^{\Delta L} \middle\| \alpha_i J_i T_i\right)^2 \qquad (8)$$

where ΔL is the transferred angular momentum (spin flip is very small and has been neglected), and $M^{(\Delta L)}(q)$ are functions of momentum transfer q which result from the DWIA integration over distorted waves and an effective zero range amplitude

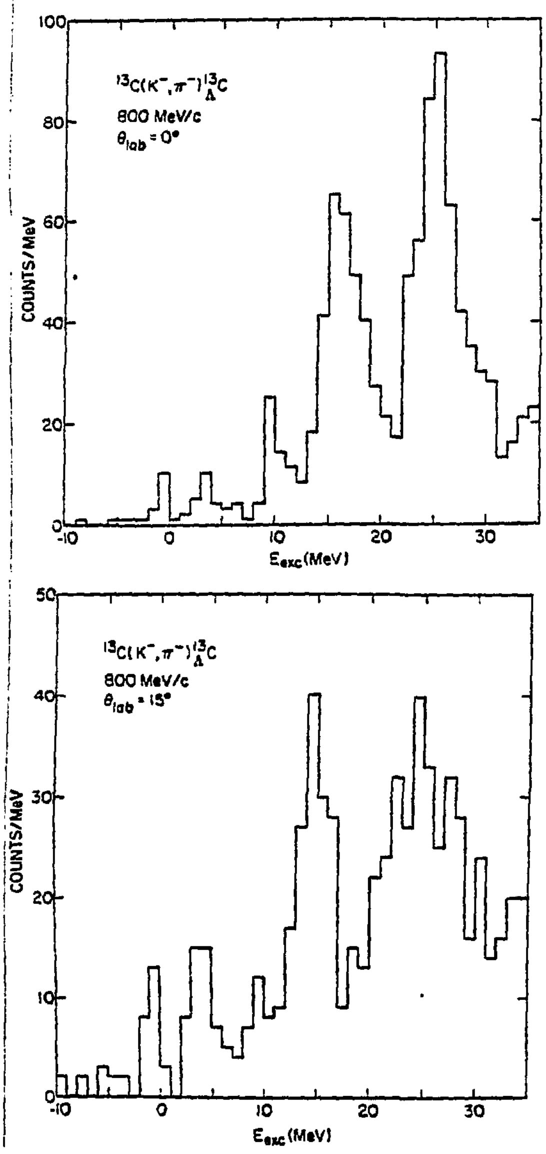

for $K^-n\to\pi^-\Lambda$. The amplitudes $M^{(\Delta L)}(q)$ peak at different q values (or equivalently, angle) and lead to the excitation of distinct final states. $M^{(0)}(q)$, which excites $1/2^-$ states in $^{13}_{\Lambda}C$ in $p_N\to p_\Lambda$ transitions, starting from the $1/2^-$ target ^{13}C, peaks at $\theta_L=0°$. The $p_N\to S_\Lambda$ transition, driven by $M^{(1)}(q)$, leads to $1/2^+$ and $3/2^+$ final states, and peaks near $\theta_L\approx 10°$ for an 800 MeV/c incident momentum. Transitions $p_N\to p_\Lambda$ also receive a contribution from $M^{(2)}(q)$, which peaks near $\theta_L\approx 15°$ here and dominates $M^{(0)}(q)$ in this angular region; $M^{(2)}(q)$ populates $3/2^-$ and $5/2^-$ final states. The $5/2^+$ and $7/2^-$ states which arise in $p_N\to S_\Lambda$ and $p_N\to p_\Lambda$ transitions (involving the coupling of the Λ to a 2^+ core excited states of ^{12}C) involve spin flip ($\Delta S=1$) for their excitation, and are produced only very weakly in the (K^-,π^-) reaction.

The theoretical spectra[25] at 4° and 15°, to be compared with the data in Figs. 2 and 3, are shown in Figs. 4 and 5. The predicted cross sections are binned as in the experiment to facilitate comparison. The contributions of each ΔL are shown separately, and display the qualitative features just discussed. In Fig. 6, we show the full angular distributions for the 10, 16 and 25 MeV peaks. The agreement of the DWIA theory and the data is very good, both in angular shapes and absolute cross sections. This gives

Fig. 2 and 3 Spectrum for the reaction $^{13}C(K^-,\pi^-)^{13}_{\Lambda}C$ at 800 MeV/c as a function of excitation energy E_{exc}, from ref. (23), for $\theta_L=0°$ (top) and $\theta_L=15°$ (bottom).

confidence in our theory of the reaction mechanism and the resulting spin assignments.

We now discuss the detailed spectroscopy of ${}^{13}_{\Lambda}C$. Some of the main features, in particular rough estimates of the energies and relative intensities of the dominant peaks, already emerge from a weak coupling picture (but, as we see later, there are important changes in some cases from residual ΛN interactions). Core excited states in ${}^{12}C$ play a crucial role in the interpretation: besides the $0^+(T=0)$ ground state of ${}^{12}C$, strong excitations in ${}^{13}_{\Lambda}C$ are seen in which the Λ couples to the $2^+(T=0)$, $1^+(T=0)$, $1^+(T=1)$ and $2^+(T=1)$ excited states of ${}^{12}C$ at 4.4, 12.7, 15.1 and 16.1 MeV, respectively. In weak coupling, the entire (K^-,π^-) cross section associated with a given core state is proportional to the neutron pickup strength, known from the reaction ${}^{13}C(p,d){}^{12}C^*$. A poor resolution experiment, which sums over groups of final states, sees just this strength.

The ΔL=1 strength seen around excitation energy 0 and 4-5 MeV corresponds to the $1/2^+$ ground state and a $3/2^+$ state obtained by coupling the $S_{1/2}$ Λ to the ${}^{12}C$ ground state and $2^+(T=0)$ state at 4.4 MeV, respectively. The peak around 10 MeV is due to $p_N \to p_\Lambda$ transitions; for $\theta_L=0°$ and 15°, the $1/2^-$ and $3/2^-$ states respectively, obtained by coupling ${}_{\Lambda}P_{1/2}$ and ${}_{\Lambda}P_{3/2}$ to the 0^+ ground state of ${}^{12}C$, dominate the cross section. As we show later, the energy shift of the 10 MeV state between 0° and 15° offers a constraint on the Λ spin-orbit interaction. Between 12 and 16 MeV of excitation energy, one sees several positive parity $(1/2^+, 3/2^+)$

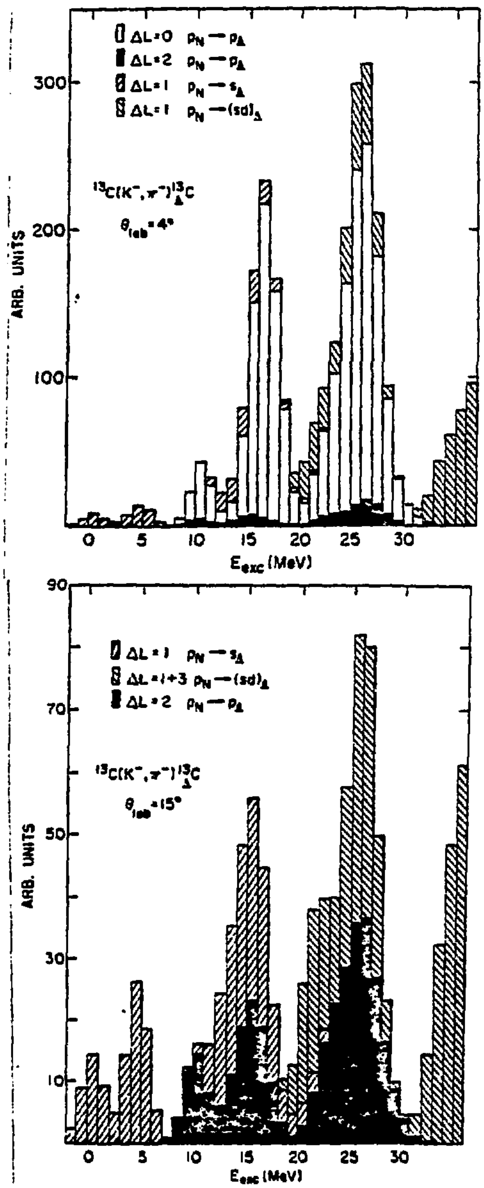

Fig. 4 and 5 Theoretical spectrum for ${}^{13}C(K^-,\pi^-){}^{13}_{\Lambda}C$ from ref. (25). The results are binned in 1 MeV intervals to facilitate comparison with the data in Fig. 2 and 3.

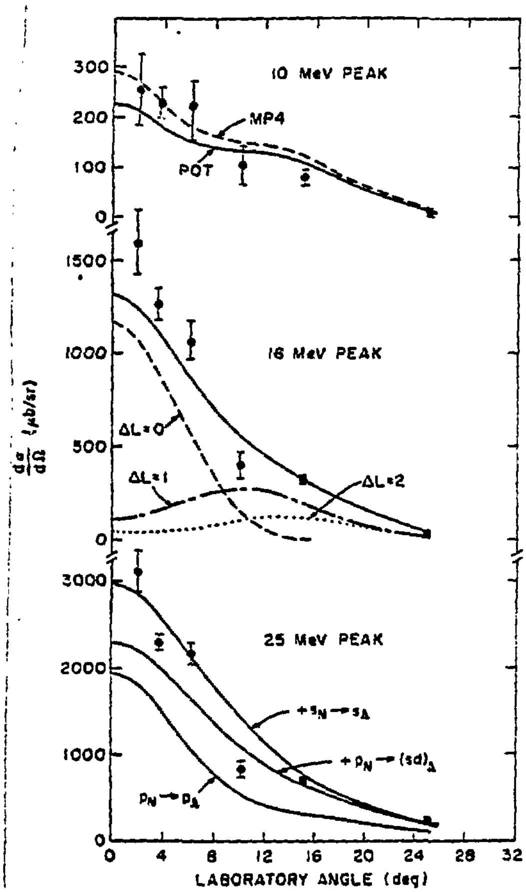

Fig. 6 Differential cross sections for the $^{13}C(K^-,\pi^-)^{13}_{\Lambda}C$ reaction at 800 MeV/c, as a function of lab angle, from ref. (25). The cross sections to the main peaks at 10, 16 and 25 MeV excitation energy in $^{13}_{\Lambda}C$ are shown, together with the data from ref. (23).

states obtained by coupling $_{\Lambda}s_{1/2}$ to core excited states of ^{12}C. The $3/2^+$ states represent a significant fraction of the strength in the 16 MeV peak at 15°. The rest of the 16 MeV strength at 15° is mostly due to two $5/2^-$ states (ΔL=2) obtained by coupling $_{\Lambda}p_{1/2,3/2}$ to the $2^+(T=0)$ core state at 4.4 MeV. At 4°, in contrast, the $1/2^-$ from $_{\Lambda}p_{3/2}$ coupled to $2^+(T=0)$ is dominant (ΔL=0). The 25 MeV peak encompasses many states arising from the coupling of $_{\Lambda}p_{1/2,3/2}$ to core states in the 13-16 MeV excitation region in ^{12}C. At 0°, ΔL=0 is largest and we see mostly $1/2^-$ states from $_{\Lambda}p_{3/2}$ coupled to $J^{\pi}=1^+$ and 2^+ cores. At 15°, the $3/2^-$ and $5/2^-$ members are seen via ΔL=2, but there are also sizable contributions from $p_N \to (sd)_{\Lambda}$ transitions with ΔL=1,3.

The interesting physics of $^{13}_{\Lambda}C$ is revealed in the deviations of the energies and relative intensities from the naive weak coupling picture. These differences are generated by the ΛN residual interaction $V_{\Lambda N}$, which we take to have the phenomenlogical form

$$V_{\Lambda N}(\underset{\sim}{r}_N-\underset{\sim}{r}_{\Lambda}) = V_o(\underset{\sim}{r}_N-\underset{\sim}{r}_{\Lambda})(1-\epsilon+\epsilon P_x)(1+\alpha\underset{\sim}{\sigma}_N\cdot\underset{\sim}{\sigma}_{\Lambda}) + V_{\pm}(\underset{\sim}{r}_N-\underset{\sim}{r}_{\Lambda})(\underset{\sim}{\sigma}_{\Lambda}\pm\underset{\sim}{\sigma}_N)\cdot\underset{\sim}{\ell}_{N\Lambda} \quad (9)$$

In addition to two-body symmetric and antisymmetric spin-orbit potentials $V_{\pm}$, we have introduced a one-body spin-orbit term for the Λ, as in Eq. (1). We expand the central part $V_o(\underset{\sim}{r}_N-\underset{\sim}{r}_{\Lambda})=\sum_{k=0}^{\infty} V_k(r_N,r_{\Lambda})P_k(\cos\theta_{\underset{\sim}{r}_N,\underset{\sim}{r}_{\Lambda}})$ and define the usual Slater integrals[27] $F^{(k)}=\int R^2_{\ell_N}(r_N)R^2_{\ell_{\Lambda}}(r_{\Lambda})V_k(r_N,r_{\Lambda})dr_N dr_{\Lambda}$. For $\ell_N=1$, $\ell_{\Lambda}=1$ we have only $F^{(0)}$ and $F^{(2)}$; the latter reflects the quadrupole part of the ΛN potential. The spin-orbit potential gives rise to a splitting $\epsilon_{p_{1/2}}^{\Lambda}-\epsilon_{p_{3/2}}^{\Lambda}=\epsilon_p$. In the present calculation[25], we assume[28] $F^{(0)}=-1.16$ MeV, $\alpha=-0.1$, $\epsilon=0$ and study the $^{13}_{\Lambda}C$ spectrum as a function of $F^{(2)}$ and ϵ_p. The energy differences of the observed peaks differ from naive predictions based only on the energies of core states, allowing us to constrain ϵ_p and $F^{(2)}$.

In the absence of an interaction of σ_Λ with the nuclear core, the lowest $1/2^-$ and $3/2^-$ states of ${}^{13}_{\Lambda}C$, obtained mainly by coupling ${}_{\Lambda}P_{1/2,3/2}$ to the 0^+ ground state of ${}^{12}C$, would be degenerate. Independent of $F^{(2)}$, the small shift[23] $\Delta E = 0.36 \pm 0.3$ MeV in the 10 MeV peak between 0° ($1/2^-$ dominant) and 15° ($3/2^-$) constrains the combination of one and two-body spin-orbit potentials to be small. If we choose $V_\pm = 0$, a value $\varepsilon_p \gtrsim 0.5$ MeV is likely, as shown in Fig. 7, while if we use a pure two-body spin-orbit force, a slightly larger ε_p is favored. This example provides a particularly clean test of the Λ spin-orbit strength. These conclusions are consistent with those of the CERN group[5,6] based on ${}^{16}_{\Lambda}O$, i.e., the Λ spin-orbit strength is very small but likely of the same sign as that for the nucleon. A better value for the Λ spin-orbit coupling is in principle obtainable from the $(K^-,\pi^-\gamma)$ reaction. The E1 γ-rays from the $1/2^-$ and $3/2^-$ levels lead to the ground state of ${}^{13}_{\Lambda}C$, but with isotropic and $1-0.6\cos^2\theta$ angular distributions[42], respectively.

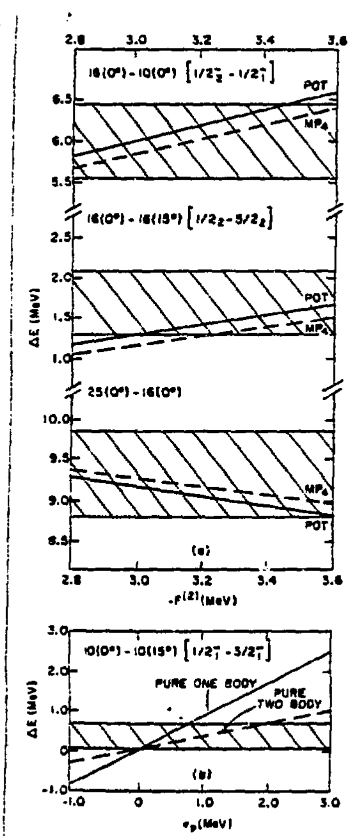

Using $\varepsilon_p = 0.5$ MeV, $V_\pm = 0$, we may now use other energy differences to constrain $F^{(2)}$. The results are shown in Fig. 7. The shift $\Delta E = 1.7 \pm 0.4$ MeV of the 16 MeV peak between 0° and 15°, if we subtract the $p_N \cdot S_\Lambda$ strength, yields a $1/2^- - 5/2^-$ splitting (same $2^+(T=0)$ core state) generated by $F^{(2)}$. The splitting of the 16 and 25 MeV peaks at 0°, both dominated by $1/2^-$ states with ${}_{\Lambda}P_{3/2}$, is less (9.3 MeV) that the naive estimate of 11.7 MeV based on the $2^+(T=0)$ and $2^+(T=1)$ core states. This is also due to $F^{(2)}$. In both cases, the data can be accounted for by using -3.4 MeV$< F^{(2)} < -3$ MeV; this value is close to the value of $F^{(2)}$ extracted from the 0° ${}^{9}_{\Lambda}Be$ spectrum by Dalitz and Gal[28].

The most interesting aspects of the ${}^{13}_{\Lambda}C$ spectrum are the energy splitting ΔE and intensity ratio R of the 16 and 10 MeV peaks at 0°. Here, the weak coupling basis states $|0^+(T=0)\otimes {}_{\Lambda}P_{1/2}\rangle_{1/2^-}$ and $|2^+(T=0)\otimes {}_{\Lambda}P_{3/2}\rangle_{1/2^-}$ are significantly mixed by $F^{(2)}$. If we write

$$|1/2^-\rangle_1 = \alpha|0^+\otimes_\Lambda P_{1/2}\rangle - \beta|2^+\otimes_\Lambda P_{3/2}\rangle \qquad (10)$$

then

$$R = (\beta\theta(1/2) + \alpha\theta(3/2))^2/(\alpha\theta(1/2) - \beta\theta(3/2))^2,$$

where $\theta(1/2)$ and $\theta(3/2)$ are the spectroscopic amplitudes for neutron pickup from the ${}^{13}C$ ground state to the first 0^+ and 2^+ states of ${}^{12}C$, respectively. With no mixing, and using Cohen-Kurath wave functions[29], one obtains R=1.8. The experimental value[23] is $R \gtrsim 5$, while the theoretical values one obtain with mixing ($\alpha \gtrsim 0.96, \beta \gtrsim 0.28$, $F_2 \gtrsim -3$ to -3.5 MeV) are $R \gtrsim 6-7$. If one makes ε too large, R increases to unacceptably large values.

Fig. 7 The top three curves show the energy splitting between various states in ${}^{13}_{\Lambda}C$, as a function of the matrix element $F^{(2)}$ of the ΛN interaction, for Λ spin-orbit splitting $\varepsilon_p = 0.5$ MeV. In the bottom figure, we show the energy difference ΔE between the "10 MeV" peak in ${}^{13}_{\Lambda}C$, seen at 0° and 15°, as a function of ε_p for fixed $F^{(2)}$.

Despite the relatively weak ΛN force, the hypernucleus displays a tendency to seek a higher degree of spatial symmetry in the lowest $1/2^-$ state. If instead of the weak coupling basis, we used the states of [54] and [441] symmetry, the first $1/2^-$ is dominately the [54] symmetry, which is forbidden by the Pauli principle for a system of nucleons. In the limit where [54] symmetry is exact for this $1/2^-$ state, one has a dynamical selection rule inhibiting its population in the (K^-,π^-) reaction, since a [54] symmetry is unreachable with $\Delta L=0$, starting with the dominant [441] of the ^{13}C ground state. This tendency towards spatial symmetry (increased by using $\varepsilon>0$) accounts for the strong deviation of R from its pick-up value in the weak coupling limit.

The full exploitation of the structure information available from Λ-hypernuclear spectra clearly requires a considerable improvement in energy resolution, available only with more intense K^- beams. As indicated here, however, one already obtains non-trivial constraints on ε_p and $F^{(2)}$ from the coarse resolution data.

4. The physics of Σ-hypernuclei

The first evidence for relatively narrow Σ states in nuclei was reported by the CERN group[30]. They studied the forward production of Σ's in the $(K^-,\pi^\pm)$ reaction at 720 MeV/c. Targets of ^6Li, ^7Li, ^9Be, and ^{12}C were used. The clearest evidence for narrow Σ structures was seen in the $^9Be(K^-,\pi^-)^9_\Sigma Be$ data, reproduced in Fig. 8. The data for the same process in the Λ region are also shown. More recently, the reaction $^6Li(K^-,\pi^+)^6_\Sigma H$ at 713 MeV/c was studied[31] at the Brookhaven AGS. The preliminary 4° spectrum in the Σ region is shown in Fig. 9. There is clear evidence for two peaks superimposed on a quasielastic background. An experiment on $^{16}O(K^-,\pi^+)^{16}_\Sigma C$ at 720 MeV/c has just been completed at the AGS, but the data have not yet been analyzed[32]. Further Σ experiments at CERN are expected in the near future[33], using a redesigned low momentum K^- beam. These experiments[33] should provide considerable impetus to the study of Σ-hypernuclei, since at 450-500 MeV/c one is much closer to the "magic momentum" of 300 MeV/c for which the momentum transfer $q=0$ for $\theta_L=0°$; the coherent substitutional Σ states (which should also be the narrowest, as we indicate later) should emerge from the quasielastic background in a more striking fashion than seen in Figs. 8 and 9 at a higher incident momentum.

There have been several theoretical approaches[19,34-36] to the problem of the width of Σ-hypernuclear states. The widths of the Σ-nuclear states seen in the $(K^-,\pi^\pm)$ reaction are related in an optical model picture to the shifts and widths of the Σ^--atomic states seen in x-ray experiments. These have been analyzed by Batty et al[37] in terms of a complex Σ optical potential of the from

$$V_\Sigma(r) = -U(r) - iW(r) = -\frac{4\pi}{2\mu}(1+m_\Sigma/m_N)b\rho(r) \tag{11}$$

where μ is the Σ-nucleus reduced mass, ρ(r) is the nuclear density, and

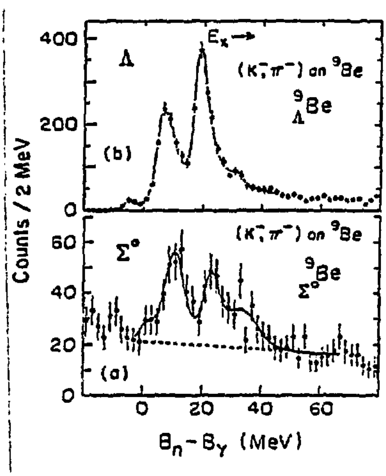

Fig. 8 Data at $\theta_L=0°$ on the reaction $^9Be(K^-,\pi^-)^9_{\Lambda,\Sigma}Be$ at 720 MeV/c from ref. (30).

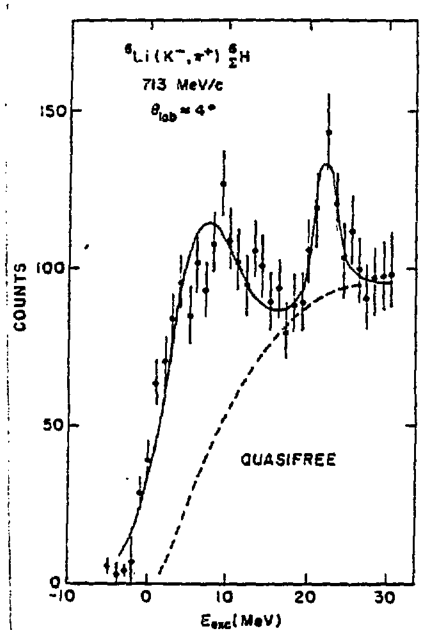

Fig. 9 The spectrum of $^6_\Sigma$H, as seen in the ^{6}Li(K$^-$,π^+)$^6_\Sigma$H reaction at 713 MeV/c, θ_L=4°. The solid curve represents a fit to the data with two Breit-Wigner resonances plus the quasielastic background shown as a dashed line, from ref. (31).

b=0.35±0.04+i(0.19±0.03)fm. The well depth in nuclear matter is then U(0)=28±3 MeV, W(0)=15±2 MeV. Deeply bound Σ states in a heavy nucleus have a single particle Σ→Λ conversion width of the order of Γ≈2W(0)≈30 MeV. In light nuclei, and for Σ levels with small binding, the optical model widths can be considerably less.

The problem of relating W(r) for the Σ to the underlying ΣN→ΛN conversion process, with inclusion of the Pauli, dispersion and binding effects due to the nuclear medium, has been considered by several authors[19,35,36]. The Pauli effects are found to suppress the ΣN→ΛN coupling in nuclear matter significantly (25% or so). Dispersive and off-shell effects are also included by summing ladder graphs for the ΣN effective interaction, using modified hyperon and nucleon propagators in the medium. In ref. (36), a particularly simple discussion is given, which shows how one can understand W(0) in terms of the free space Σ→Λ conversion cross section, if medium corrections are included.

A thorough study of Σ hypernuclear states, based on the phenomenological Σ^- potential of Eq. (11), has been given by Gal, Toker and Alexander[36]. They suggest that normalizable Σ unstable bound states (sometimes embedded in the Σ continuum) are seen in the (K$^-$,π) process. The properties of these states are studied in detail, in order to identify relatively narrow (Γ<10 MeV) candidates. They argue that the Σ continuum states observed in (K$^-$,π) reactions are unlikely to be of the usual (nonnormalizable) Gamow type. In Fig. 10, we show results[36] for 1S and 1P unstable bound states (UBS) in the system $^{13}_\Sigma$C. The binding energy B and width Γ vary within the four-sided figures as one varies the complex depth of the phenomenological Σ^- potential within its error bars. We see that the 1S state in $^{13}_\Sigma$C is always broad but that the 1P UBS could be as narrow as 6 MeV in the optical model. In the case of $^9_\Sigma$Be, it is shown[36] that the 1P UBS has a width of only 3-4 MeV if it lies 8 MeV in the Σ continuum, corresponding approximately to the lower Σ peak in Fig. 8. Thus it is possible for narrow Σ states to arise in the optical model, in contrast to one's naive intuition based on the estimate Γ=2W(0).

The optical model picture presented above neglects an important feature of ΣN→ΛN conversion, namely its spin-isospin selectivity[34]. At low momentum the dominant contribution to conversion arises from the $^3S_1$, I=1/2 partial wave[16]. Dynamically, this arises because of the ΣN initial state interactions, which are strongly attractive for $^3S_1$, I=1/2 and repulsive for $^1S_0$, I=1/2. The attraction focuses the wave function, so that conversion takes place more easily. In addition, the tensor part of π and ρ exchange is kinematically favored in the 80 MeV ΣN→ΛN conversion.

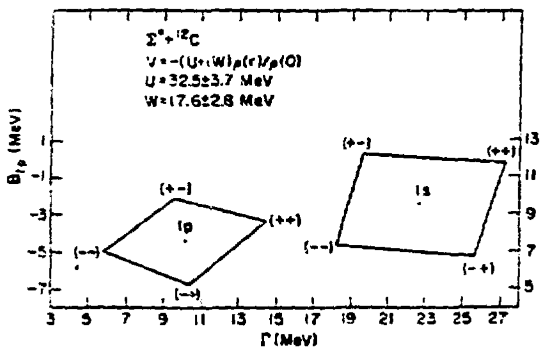

Fig. 10 Calculated (ref. 36) binding energies $B_{1S,1P}$ and widths Γ of normalizable $\Sigma^{\circ}+{}^{12}C$ states in the optical potential V shown in the figure. The central points correspond to using U=32.5 and W=17.6 MeV. The four corners labeled (±±) represent the effect of varying U and W up to the error bars in either direction.

In heavy nuclei, where spins and isospins are close to saturation, this selectivity has little consequence. For light systems, its effects are more pronounced. In its simplest form, the expectation value of the transition operator $\sum_i \delta(\underline{r}_i - \underline{r}_\Sigma)$ which occurs in the optical model must be replaced by $1/12\sum_i \delta(\underline{r}_i - \underline{r}_\Sigma)(3+\underline{\sigma}_i \cdot \underline{\sigma}_\Sigma)(1-\underline{\tau}_i \cdot \underline{\tau}_\Sigma)$. This operator is to be sandwiched between hypernuclear wave functions which depend explicitly on spin and isospin. Depending on the total spin J and isospin I of the Σ hypernuclear levels, as well as the details of the coupling scheme, one obtains widths which are sometimes quenched and sometimes increased with respect to the optical model limit.

The most dramatic effects ot selectivity are found for 0^+ states of maximum isospin formed by the coherent replacement $(\ell j)_N \to (\ell j)_\Sigma$. For example, in a simple j-j coupling picture of ${}^{12}_{\Sigma}C$, the width of the coherent $(NP^{-1}_{3/2} \otimes \Sigma P_{3/2})_{0^+, I}$ states changes significantly from the nuclear matter value $\Gamma = \Gamma_s + \Gamma_p$ to $\Gamma(0^+, I=1/2) = \Gamma_s + 12/7\Gamma_p$ and $\Gamma(0^+, I=3/2) = \Gamma_s$. For the I=3/2 state, the Σ^- annihilation on P-shell nucleons is totally suppressed by the presence of spin-isospin correlations in the initial j-j hypernuclear wave function. The quenching factor $\Gamma_s/\Gamma_s+\Gamma_p$ assumes the value 0.41 if one uses oscillator wave functions, so a total width of the order of 5 MeV might be anticipated for the 0^+,I=3/2 excitation in ${}^{12}_{\Sigma}Be$, if one uses the optical model width of 11.4 MeV for the 1p state obtained in ref. 36).

Other examples of selectivity involving ${}^7Li$, ${}^9Be$ and ${}^{16}O$ targets are discussed in ref. (34). In a simple LS coupling model, tentative quantum number assignments are given for the two peaks observed in the ${}^9_{\Sigma}Be$ spectrum of Fig. 8. These are suggested to be 0^+ states involving the coherent transition $1P_N \to 1P_\Lambda$, with $(S_N, I_N, I) = (0,0,1)$ and (1,1,2) for the lower and upper peak, respectively, where (S_N, I_N) are the ${}^8Be$ core spin and isospin. This simple picture may be altered by the strong spin dependence of the ΣN residual interaction, which would mix the (1,1,2) and (0,1,2) configurations, for instance. Note that of the two peaks seen in the ${}^9Be\,(K^-,\pi^-){}^9_{\Sigma}Be$ spectrum, only the upper I=2 peak is predicted to be seen in the ${}^9Be\,(K^-,\pi^+){}^9_{\Sigma}He$ reaction, which acts as an isospin filter.

The s-shell targets ${}^3He$ and ${}^4He$ also offer interesting possibilites[38] for narrow Σ states, although no experiments have yet been attempted. In the reaction ${}^4He(K^-,\pi^-){}^4_{\Sigma}He$, for instance, one can populate two 0^+ states with I=1/2 or 3/2 from the $S_N \to S_\Lambda$ transition. Selectivity makes an enormous difference in the width of these states: the I=1/2 state is predicted to have twice the optical model width, while the I=3/2 member has essentially no Σ-Λ conversion width. To see this, consider the ${}^4He(K^-,\pi^+){}^4_{\Sigma}n$ reaction to the I=3/2 state. The initial pp pair is in a ${}^1S_0$ state; after a coherent substitution $p \to \Sigma^-$, the resulting Σ^-p pair remains as ${}^1S_0$. Since Σ^-n cannot convert and Σ^-p converts dominately in ${}^3S_1$, the width of the I=3/2 state should be small. The problem in observing such a state is that it may well lie fairly high in the Σ continuum. Since it corresponds to an

S-wave, it cannot exist as a conventional single particle resonance. However, it may survive as a normalizable UBS in the Σ continuum, of the type discussed by Gal et al.[36].

The case of $^6Li(K^-,\pi^+)^6_\Sigma H$ provides the best test of the selectivity mechanism to date. The data shown in Fig. 9 display two distinct peaks, at roughly 7 and 22 MeV of excitation energy. The upper peak is seen to be narrower, with a width of 3 MeV consistent with the experimental resolution. In ref. (38), these data are given a *quantitative* interpretation in terms of $P_N \to P_\Sigma$ and $P_N \to S_\Sigma$ transitions (lower peak) and the $S_N \to S_\Sigma$ transition (upper peak). Since the S_N^{-1} hole strength in ^6Li is known to be dominated by a very narrow ($\Gamma \approx 100$ keV) ^5He $3/2^+$ excited state at 16.76 MeV, coupling a Σ in the 1S to this core state to form 1^+ produces a narrow state, in analogy to a similar $S_N \to S_\Lambda$ transition observed[39] in $^6_\Lambda Li$, and interpreted[40] in a cluster model. For Σ^-, the cluster decomposition expected for this state is

$$\left[{}^4_\Sigma n(I=3/2,\ I_3=-3/2, S=0) \otimes d\right]_{1^+} \qquad (12)$$

Since $^4_\Sigma n$ has the structure $^4_\Sigma n = (\Sigma^- p)_{S=0}(nn)_{S=0}$, the Σ^- can only convert to Λ on the proton in the deuteron cluster, and the width remains small.

In ref. (38), angular distributions for the reaction $^6Li(K^-,\pi^+)^6_\Sigma H$ at 720 MeV/c are calculated in the eikonal DWIA approximation. Typical results are shown in Fig. 11. The ratio of cross sections in the two peaks is consistent with the data in Fig. 9. A very similar calculation[38] for $^6_\Lambda Li$, with the same choices for optical potentials and the geometry of the nucleon and hyperon single particle wells, yielded good agreement in both absolute cross section and angular shape with the CERN data[39] for the $S_N \to S_\Lambda$ transition. The cross section for the lower bump is summed over all states arising from $P_N \to S_\Lambda$ and $P_N \to P_\Sigma$ transitions. Since $q \gtrsim 130$ MeV/c is rather sizable even for $\theta_L = 0°$, the $P_N \to S_\Sigma$ process to a complex of negative parity levels is non-negligible, accounting for about 60 μb/sr at 4° in Fig. 11. The coherent $P_N \to P_\Sigma$ transition ($\Delta L=0$), leading to a 1^+ level (dominantly $^3S_1$), yields a sharply falling angular distribution. The incoherent $P_N \to P_\Sigma$ transition ($\Delta L=2$) leads in the LS limit to a $1^+, 2^+, 3^+$ triplet (^3D_J) with branching ratios $2J+1$. The $\Delta L=2$ part is non-negligible ($\gtrsim 35$ μb/sr) even at 0°, and exceeds the $\Delta L=0$ strength above 6° or so. The ^3D levels are expected to have a width comparable to that of the $^3S_1$ state; their mean position should lie some 2-3 MeV higher than $^3S_1$. Thus the lower bump in Fig. 9 reflects the presence of several Σ-hypernuclear states; the apparent width then

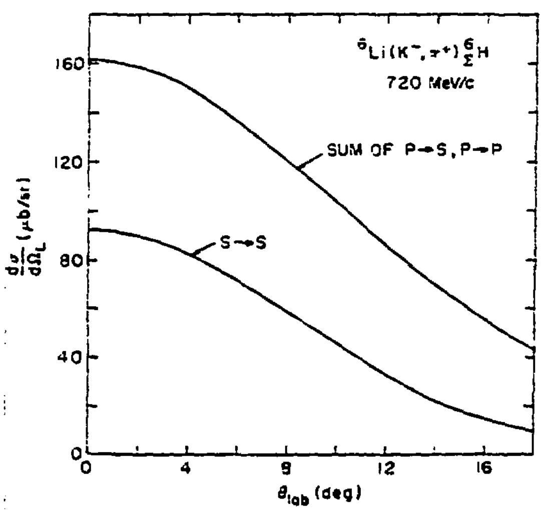

Fig. 11 Theoretical angular distributions, from ref. (38), for the reaction $^6Li(K^-,\pi^+)^6_\Sigma H$ at 720 MeV/c. The curve labeled S→S corresponds to the narrow upper peak in Fig. 9, while the summed P→S, P→P curve is to be associated with the total strength in the lower peak of Fig. 9.

arises from resolution and energy splittings ($P_\Sigma - S_\Sigma$, ${}^3S_1 - {}^3D_J$) as well as the intrinsic Σ width.

The role of the ΣN residual interaction has been ignored in the simple considerations we have presented thus far. Unlike the ΛN interaction, the ΣN potential exhibits strong spin and isospin dependence (attractive for ${}^1S_0$, I=3/2 and ${}^3S_1$, I=1/2 and repulsive for ${}^1S_0$, I=1/2 and ${}^3S_1$, I=3/2). In the Σ central potential, these channels appear with the ordinary statistical weights (2S+1)(2I+1), resulting in a well depth $V_{0\Sigma}$ somewhat shallower than for the Λ. When considered as a residual interaction, on the other hand, say connecting $N^{-1}\Sigma$ particle-hole states, the ΣN force enters with different weights depending on the coupling scheme. In some cases, <u>coherent shifts</u> of Σ-hypernuclear states occur. For instance, in ${}^{12}_{\Sigma}C$ and ${}^{16}_{\Sigma}O$, the relatively narrow 0^+, I=3/2 states are shifted upwards, while the 0^+, I=1/2 states enjoy a significant downward shift. Smaller effects are found for 1^- and 2^+ states. Thus for the Σ, there may be very interesting (and strong) deviations from the weak coupling limit. However, it will be difficult to develop a phenomenology of ΣN effective interactions unless a number of narrow states are seen. The experiments to date are tantalizing, but one requires more data on a variety of targets, particularly angular distributions for the lowest possible K^- momentum. As we have indicated, the widths of Σ levels, as well as their energies and relative cross sections in the ($K^-,\pi^\pm$) reactions, are sensitive indicators of the degree of configuration mixing induced by the ΣN interaction. Exciting prospects for Σ-hypernuclear physics lie ahead.

5. Future directions for hypernuclear research

There are several other proposals for experiments in hypernuclear physics which are either approved or under active consideration. We review here the physics motivations for some of these proposals.

The planned CERN experiments[33] on the formation of Σ-hypernuclei with a 450-500 MeV/c K^- beam have already been mentioned. These low momentum experiments are crucial, for they will optimize the formation of <u>coherent</u> substitutional Σ states by reducing the background due to quasielastic processes. Since we expect[34] the coherent Σ states of maximum isospin I_{max} to be the narrowest, the (K^-,π^+) reaction is more favorable than (K^-,π^-), since the latter will contain contributions from broader excitations with lower isospin.

The ($K^-,\pi^-\gamma$) reaction was mentioned earlier, in connection with the decay of certain states in ${}^{13}_{\Lambda}C$, which may enable us to determine the Λ spin-orbit splitting with much greater precision. A ($K^-,\pi^-\gamma$) experiment[41] is approved for the Brookhaven AGS. The role of the γ ray measurements in elucidating hypernuclear structure has been discussed by Dalitz and Gal[42]. A central point is that even if one cannot obtain good energy resolution on the π^-, the γ energy can be measured with precision. One then obtains <u>energy differences</u> of levels accurately, which can be used to more tightly constrain the ΛN interaction. The (K^-,π^-) reaction significantly populates only natural parity levels ($0^+,1^-,2^+$ etc.) starting with a spin zero target. The subsequent γ ray emission, however, also populates some of the <u>unnatural parity</u> levels. In some favorable cases, one may be able to detect the M1 γ ray connecting the two members of the ground state doublet ($2^- \to 1^-$ in ${}^{12}_{\Lambda}C$, for instance). A knowledge of the energy splitting would enable us to quantitatively determine the spin dependence of the effective ΛN interaction in the $1S_\Lambda$ "state". Transitions from levels with $\ell_\Lambda \neq 0$ constrain the spin-orbit terms in Eq. (9).

Another fascinating subject of study concerns the weak decay modes of hypernuclei. An approved experiment[43] for the AGS will measure the lifetime and the rates for π^- and p emission in the weak decay of ${}^{12}_{\Lambda}C$. In a hypernucleus, the free decay modes $\Lambda \to p\pi^-, n\pi^0$ are suppressed by the Pauli principle, since the recoiling nucleon has only 5 MeV of energy. On the other hand, the presence of nuclear matter introduces non-mesonic decay modes $\Lambda p \to np$ and $\Lambda n \to nn$, involving the emission of energetic nucleons. The hypernucleus provides a unique laboratory for the study of such four fermion weak interactions.

Recently, the (π,K) reaction has been suggested[44] as a possibility for the production of hypernuclei, and an experiment is planned[45] for the AGS. Some preliminary (π,K) runs[45] with nuclear targets have also been carried out at CERN. Since the momentum transfer q in the associated production reaction $\pi^+ n \to K^+ \Lambda$ is large (>300 MeV/c for $p_\pi \lesssim 1.2$ GeV/c), the (π,K) reaction on nuclei will preferentially populate high spin states. This complements nicely the (K^-,π^-) studies at low q, which emphasize low spin configurations. In a simple Λ particle, n hole picture, the largest (π,K) cross sections are to natural parity "stretch" states with $J = \ell_n + \ell_\Lambda$.

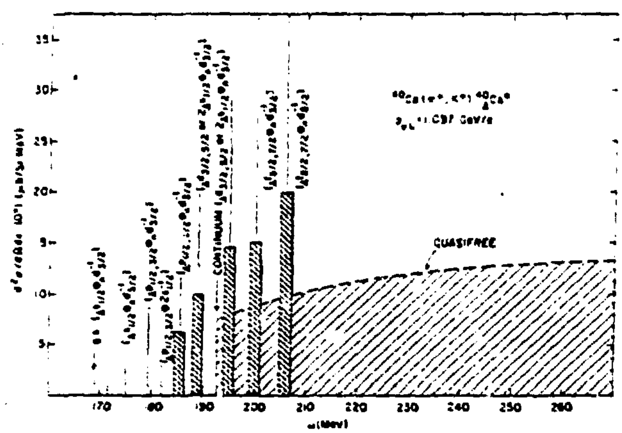

Fig. 12 Predicted excitation spectrum of ${}^{40}_{\Lambda}Ca$, as seen at 0° in the (π^+,K^+) reaction at 1.1 GeV/c, from ref. (44). The high spin states near or above the Λ continuum are arbitrarily given a width of 2 MeV.

In Fig. 12, we show a predicted[44] spectrum for the process ${}^{40}Ca(\pi^+,K^+){}^{40}_{\Lambda}Ca^*$ at 1.1 GeV/c. The largest cross sections are to 4^+ and 5^- states arising from the $d_N \to d_\Lambda$ and $d_N \to f_\Lambda$ single particle transitions; the f_Λ orbit lies in the continuum, so the 5^- level may be quite broad. The population of the 2^+ ground state of ${}^{40}_{\Lambda}Ca$ is weak, since J and q are mismatched. The quasifree spectrum for (π^+,K^+) is very flat as a function of excitation energy unlike the (K^-,π^-) reaction, since q is large.

One can also contemplate the production of Σ hypernuclei; this would be best done via the (π^-,K^+) reaction.

As a final topic of the "futuristic" sort, we mention the possibility[46] of producing Ξ^- or $\Lambda\Lambda$ hypernuclei of strangeness S=-2 with the (K^-,K^+) reaction. Such studies would shed light on the $\Lambda\Lambda$ and ΞN interactions at low energies, thereby extending our knowledge of the SU(3) structure of baryon-baryon forces. The elementary process $K^- p \to K^+ \Xi^-$ is backward peaked, so the (K^-,K^+) cross sections on nuclei near $\theta_L = 0°$ are very small (a few hundred nb/sr in the most favorable cases). Since q is large, high spin Ξ states will be favored.

In Fig. 13, we display a predicted[46] spectrum for the reaction ${}^{28}Si(K^-,K^+){}^{28}_{\Xi}Mg$ at 1.26 GeV/c. It should be emphasized that these results are highly speculative: one has no reliable empirical knowledge of the Ξ's real potential in a nucleus, or its conversion width via $\Xi^- p \to \Lambda\Lambda$. Even the sign of the real part is uncertain (see section 2), although it is probably weakly attractive (we assume a depth $V_{0\Xi} = 15$ MeV in Fig. 13). In analogy with the case of Σ hypernuclei, we expect that narrow Ξ states exist at least in some light systems. Some of the Ξ states can also benefit from the selectivity mechanism discussed earlier for Σ's, since the low energy $\Xi^- p \to \Lambda\Lambda$ conversion must proceed from the ${}^1S_0$, I=0 channel of $\Xi^- p$. The width of the high spin states populated in (K^-,K^+) are very little effected by selectivity, however[46]. One eagerly awaits experiments which could reveal the predicted rich spectroscopy of doubly strange hypernuclei.

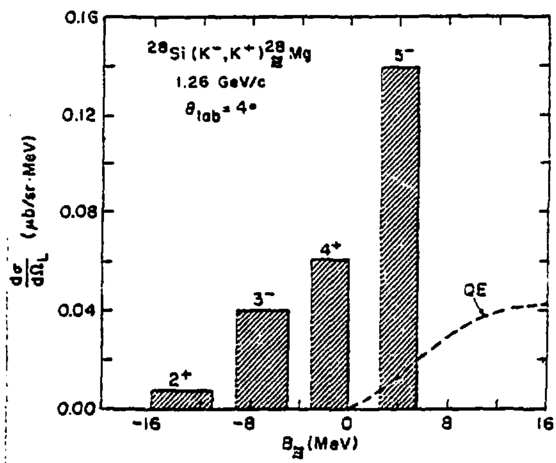

Fig. 13 Hypothetical 4° spectrum of the doubly strange hypernucleus $^{28}_{\Xi}Mg$, produced in the (K^-,K^+) reaction at 1.26 GeV/c, from ref. (46). An attractive real potential of depth 15 MeV, plus a Coulomb potential, was assumed for the Ξ^-. Widths of 5, 4, 3 and 3 MeV are arbitrarily assigned to the states involving a Ξ^- in a s,p,d,f orbit, respectively. The highest natural parity spin state, which dominates the cross section, is indicated for each peak.

I would like to thank Avraham Gal for a careful reading of the text, and for numerous discussions on the presentation of the material given here, much of which is taken from our joint work. I have also benefitted from discussions with S. Kahana and D. J. Millener. This work was supported by the U.S. Department of Energy under Contract No. DE-AC02-76CH00016.

References

1. A. Gal, in Advances in nuclear physics, eds. M. Baranger and E. Vogt, vol. 8 (Plenum Press, New York, 1975), p. 1.
2. B. Povh, Rep. Prog. Phys. 39 (1976) 824; in Ann. Rev. Nucl. Part. Sci., eds. J. D. Jackson, H. E. Gove and R. F. Schwitters, vol. 28 (Annual Reviews, Inc., Palo Alto, 1978) p. 1; Nuclear physics with hyperons, Max Planck Institute preprint MPI H-1979-V25 (1979).
3. R. Dalitz, Proc. Int. Conf. on nuclear physics, Berkeley, 1980, eds. R. M. Diamond and J. O. Rasmussen (North-Holland, Amsterdam, 1981) p. 101.
4. C. B. Dover, Proc. Int. Topical Conf. on meson-nuclear physics, Houston, 1979, ed. E. V. Hungerford (American Institute of Physics, New York, 1979) p. 634; Proc. Kaon Factory Workshop, Vancouver, 1979, ed. M. K. Craddock (TRIUMF report TRI-79-1) p.4.
5. W. Brückner et al., Phys. Lett. 79B (1978) 157.
6. A. Bouyssy, Phys. Lett. 91B (1980) 15; note that spin-orbit potentials are defined by Bouyssy with the factor $r_0^2=(1.1)^2fm^2$ replacing $(\hbar/m_\pi c)^2=2fm^2$ in Eq. (1).
7. H. J. Pirner, Phys. Lett. 85B (1979) 190.
8. J. V. Noble, Phys. Lett. 89B (1980) 325.
9. A. Bouyssy, Phys. Lett. 99B (1981) 305.
10. R. Brockmann and W. Weise, Nucl. Phys. A355 (1981) 365.
11. G. E. Brown, private communication.

12. J. D. Walecka, Ann. of Phys. 83 (1974) 491; F. E. Serre and J. D. Walecka, Phys. Lett. 79B (1978) 10; B. D. Serot and J. D. Walecka, Phys. Lett. 86B (1979) 146.
13. M. R. Anastasio, L. S. Celenza and C. M. Shakin, Phys. Rev. C23 (1981) 2258 and 2273; L. S. Celenza, B. Goulard and C. M. Shakin, Brooklyn College preprint 81/031/106, March, 1981.
14. C. B. Dover, A. Gal and J. V. Noble, manuscript in preparation.
15. S. A. Moszkowski and B. L. Scott, Ann. of Phys. 11 (1965) 65.
16. M. M. Nagels, T. A. Rijken and J. J. deSwart, Phys. Rev. D12 (1975) 744; D15 (1977) 2547; D20 (1979) 1633.
17. R. R. Scheerbaum, Phys. Lett. 61B (1976) 151; 63B (1976) 381.
18. J. Rozynek and J. Dabrowski, Phys. Rev. C20 (1979) 1612.
19. J. Dabrowski and J. Rozynek, Phys. Rev. C23 (1981) 1706.
20. H. Bando and I. Shimodaya, Prog. Theor. Phys. 63 (1980) 1812; H. Bando, preprint (1981).
21. G. E. Brown, J. Speth and J. Wambach, Phys. Rev. Lett. 46 (1981) 1057.
22. C. D. Goodman et al., Phys. Rev. Lett. 44 (1980) 1755; D. Bainum et al., Phys. Rev. Lett. 44 (1980) 1751.
23. M. May et al., submitted to Phys. Rev. Lett.
24. R. Chrien et al., Phys. Lett. 89B (1979) 31.
25. E. H. Auerbach, A. J. Baltz, C. B. Dover, A. Gal, S. Kahana, L. Ludeking and D. J. Millener, submitted to Phys. Rev. Lett.; the $1S_\Lambda$ spectroscopy has been taken from A. Gal, J. M. Soper and R. H. Dalitz, Ann. of Phys. 113 (1978) 79.
26. R. A. Eisenstein, Nukleonika 25 (1980) 535.
27. A. de-Shalit and I. Talmi, Nuclear Shell Theory (Academic Press, New York, 1963) p. 208-209.
28. R. H. Dalitz and A. Gal, Ann. Phys. 131 (1981) 314.
29. S. Cohen and D. Kurath, Nucl. Phys. 73 (1965) 1; Nucl. Phys. A101 (1967) 1.
30. R. Bertini et al., Phys. Lett. 90B (1980) 375.
31. E. V. Hungerford, private communication (BNL-CMU-Houston-MIT-Vassar-Torino collaboration).
32. R. Chrien and M. May, private communication.
33. B. Povh, private communication; proposal CERN/PSCC/79-37.
34. A. Gal and C. B. Dover, Phys. Rev. Lett. 44 (1980) 379; ibid 962; A. Gal, Nukleonika 25 (1980) 447.
35. L. S. Kisslinger, Phys. Rev. Lett. 44 (1980) 968; W. Stepien-Rudzka and S. Wycech, Nucl. Phys. A (1981), in press; S. Wycech, W. Stepien-Rudzka and J. R. Rook, Nucl. Phys. A324 (1979) 288.
36. A. Gal, G. Toker and Y. Alexander, submitted to Annals of Physics.
37. C. J. Batty et al., Phys. Lett. 74B (1978) 27; C. J. Batty, Phys. Lett. 87B (1979) 324.
38. C. B. Dover and A. Gal, manuscript in preparation.
39. R. Bertini et al., preprint CERN-EP/81-14 (March, 1981).
40. L. Majling et al., Phys. Lett. 92B (1980) 256.
41. M. Deutsch et al., AGS proposal No. 760.
42. R. H. Dalitz and A. Gal, Ann. of Phys. 116 (1978) 167.
43. P. Barnes et al., AGS proposal No. 759.
44. C. B. Dover, L. Ludeking and G. E. Walker, Phys. Rev. C22 (1980) 2073.
45. A. Thiessen et al., AGS proposal No. 758, and private communication.
46. C. B. Dover and A. Gal, manuscript in preparation; C. B. Dover, Nukleonika 25 (1980) 521.